JOURNAL OF MATERIALS SCIENCE 29 (1994) 3691–3701

Conductivity measurements of various yttria-stabilized zirconia samples

J. VAN HERLE, A. J. McEVOY, K. RAVINDRANATHAN THAMPI
Institut de Chimie Physique II, Ecole Polytechnique Fédérale de Lausanne, 1015 Lausanne, Switzerland

Samples of yttria-stabilized zirconia manufactured by the following fabrication procedures, were obtained from commercial sources: (i) hot isostatic pressing; (ii) tape casting; (iii) vacuum plasma spraying, and (iv) calendering. The ionic conductivities of these samples were measured by (a) impedance spectroscopy; (b) the four-point probe method; (c) the current-interruption technique, and (d) the van der Pauw technique. The tape-cast and hot pressed samples showed good and very reproducible conductivity values. The vacuum plasma sprayed samples showed an anisotropy in their conductivity, with the cross-plane value being several times lower than the in-plane value. A simple model based on the porous microstructure of these samples can explain this observation. Sintering of the plasma sprayed samples minimized the anisotropy and significantly improved their conductivity values. The calendered samples also showed a similar anisotropy in their conductivity data when they were inadequately sintered.

1. Introduction

Yttria-stabilized zirconia (YSZ) is the most widely used solid electrolyte in solid oxide fuel cell (SOFC) applications [1, 2]. Despite its relatively high resistivity compared to alternative solid electrolytes, like doped CeO_2 or Bi_2O_3 [3–6], it is still used because of its superior chemical stability under extreme conditions of temperature and gas environment (oxidizing and reducing on opposite faces of electrolyte). Besides, for samples that are thin enough ($< 300\ \mu m$), its conductivity is still sufficient to allow high current densities ($> 2\ A\ cm^{-2}$), at not too low temperatures (900 °C).

YSZ is fabricated by commercial manufacturers and university laboratories in a variety of ways [1, 2, 7, 8]. Fabrication techniques include hot isostatic pressing (HIP) [9], tape casting (TC) [10–13], vacuum plasma spraying (VPS) [14–20], atmospheric plasma spraying (APS) [21, 22], sputtering [3, 23–25], calendering [26, 27], sol–gel processing [28], electrochemical vapour deposition (EVD) [29–31], chemical vapour deposition (CVD) [31, 32], vapour phase electrolytic deposition (VED) [33, 34], slurry coating [18, 35, 36], spray pyrolysis [35, 37, 38], laser physical vapour deposition (LPVD) [39–41], slip casting [36, 37, 42] and ion plating [20, 37, 43]. A partial overview of deposition techniques is covered in [44].

Solid oxide fuel cells with electrolytes that originate from one or other of these fabrication procedures may show big differences in their power output characteristics [18, 37, 45–47]. Of course, electrolyte resistivity constitutes only one of the losses that occur in a solid oxide fuel cell, and normally is not solely responsible for performance differences. Indeed, the losses occurring at the electrodes (polarization losses) are generally recognized as being more important than the pure ohmic loss of the electrolyte [48, 49]. This provides, in fact, another argument in favour of the continued use of YSZ as an electrolyte, in spite of the availability of other, better conducting (but less stable) electrolytes [3–6]. As long as electrode polarization losses are dominant in overall cell performance, little can be gained by replacing the electrolyte material.

However, one fact seems to emerge from the literature: whenever the electrolyte membrane of a test cell is not perfectly dense, the maximum obtainable output of the cell is low. On comparing experimental data of cells with a differently fabricated YSZ electrolyte with otherwise identical electrodes, this fact becomes clear [18, 45–47]. It is pronounced for cells with a YSZ electrolyte made by VPS [18, 21, 45, 46, 50], sputtering [23, 25], ion plating [37, 45, 47] or APS [21, 46]. Some values are listed in Table I.

As an example, Fig. 1 shows a current–voltage curve of a VPS cell tested in the laboratory. The maximum power output is less than $100\ mW\ cm^{-2}$ at 900 °C, whereas the envisaged working point of SOFC should be at least over $200\ mW\ cm^{-2}$ at this temperature, considering the thickness of the YSZ layer. Impedance spectroscopy measurements showed that, in this case, electrolyte resistance is responsible for 90% of the loss. This illustrates the point that electrolyte ohmic polarization can be solely responsible for poor overall cell performance.

Nevertheless, this experiment shows the high potential of the VPS technique: the high energy impact of the plasma spray produces a very intimate electrode–electrolyte contact, resulting in low electrode polarization. In fact, the high potential of plasma spraying techniques has been demonstrated,

0022–2461

TABLE I Power densities at 1000 °C reported in literature for SOFC with different YSZ electrolytes. The fabrication techniques reputed to produce porous electrolyte structures are; VPS, vacuum plasma spraying; APS, atmospheric plasma spraying. Electrodes: perovskite cathode and cermet anode

Fabrication technique	Thickness (μm)	OCV[a] (V)	Power ($W cm^{-2}$)	Reference
VPS	200	0.90	0.14	14
	n.a.[b]	0.95	0.15	15
	130	1.00	0.16	16
	n.a	0.90	0.28	17
	164	0.90	0.14	18
	120	1.10	> 0.30	19
	200	0.90	0.26	20
	150	0.97	0.95	37
	200	0.90	0.20	47
	n.a.[b]	0.90	0.05	46
APS	200	1.00	0.35	22
	n.a.[b]	0.50	0.01	46
Ion plating	2	0.50	0.02	37
	40	0.50	0.01	45
Sputtering	12	0.80	0.02	23

[a] OCV: open circuit voltage.
[b] n.a.: not available.

TABLE II Power densities at 1000 °C reported in literature for SOFC with different YSZ electrolytes. The fabrication techniques are reputed to produce dense electrolyte structures. Electrodes: perovskite cathode and cermet anode

Fabrication technique	Thickness (μm)	OCV[a] (V)	Power ($W cm^{-2}$)	Reference
Tape-casting	n.a.[b]	1.10	0.65	11
	500	1.05	0.80	13
	100	1.00	0.90	–
Calendering	n.a.[b]	1.00	0.40	26
	100	n.a.[b]	0.40	51
EVD[c]	10	1.05	1.20	13
	10	1.00	1.55	30
Slurry coating	40	1.00	0.40	35
	50	1.10	1.47	37
	50	1.00	0.40	45
Slip casting	15	1.10	0.50	36
	100	1.10	0.70	37, 42
	150	1.10	0.70	45
Spray pyrolysis	30	1.00	0.50	35, 37, 45
	33	0.96	0.50	38

[a] OCV: open circuit voltage.
[b] n.a.: not available.
[c] EVD: electrochemical vapour deposition.

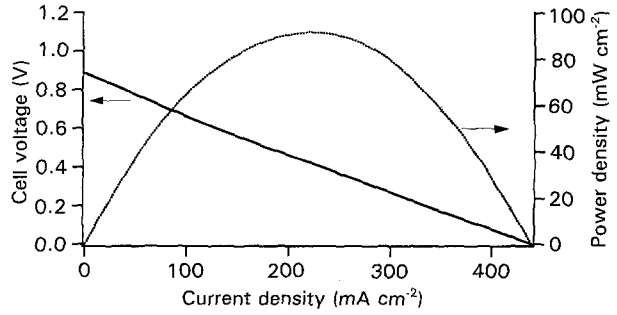

Figure 1 Current–voltage and power curve of a VPS single cell H_2–3% H_2O, Ni-cermet/YSZ (200 μm)/$La_{0.9}Sr_{0.1}MnO_3$, air at 910 °C. Electrode area 4.5 cm^2. Pt mesh current collectors.

attaining, e.g. 0.95 W cm^{-2} for VPS [37] or 0.35 W cm^{-2} for APS [22] at 1000 °C.

In general, however, power densities rarely reach 0.3 W cm^{-2} at 1000 °C when the YSZ electrolyte was fabricated by one of the "porous methods" (Table I). On the contrary, higher power densities have regularly been attained with cells where the YSZ electrolyte was dense in structure. Some values are given in Table II. In all cases the same classical electrodes, Ni-cermet anode and a perovskite cathode, or minor variants of these, were used.

A general feature of Tables I and II (and Fig. 1) is that the porosity of the electrolyte is reflected in the observed open circuit potential (OCV) of the cells. At 900–1000 °C, it lies at around 0.9 V for cells with "porous" electrolytes, whereas for cells with dense electrolytes this value was higher than 1 V.

This paper investigates the ionic conductivity of the following YSZ electrolytes: (i) thick HIP samples, which are perfectly dense; (ii) VPS samples, that are liable to be porous; (iii) tape-cast and (iv) calendered samples, both for which an optimal sintering process of the "green films" is obviously crucial for total densification.

Preliminary measurements showed that it was important to measure the conductivity of the samples in two directions (Fig. 2), denoted "in-plane" and "cross-plane", the latter being more relevant to SOFC operation. Cross-plane conductivity was measured by impedance spectroscopy and/or by the current-interruption technique, whereas in-plane conductivity was determined by the classical four-point method or, alternatively, by the van der Pauw method.

2. Experimental procedure

2.1. YSZ electrolyte samples

Table III gives an overview of the origin, dimensions and composition of the different YSZ samples used in this study.

2.1.1. Conductivity and phase

Since 6 mol % YSZ (6YSZ) is of a composition that lies at the lowest limit of the purely cubic phase domain [52, 53], it was checked, by X-ray diffraction whether any other phase (monoclinic, tetragonal) was present as an impurity in significant amounts, since this inherently affects the conductivity of the sample. X-ray diffraction of the 6YSZ HIP sample showed that all the reflections observed were due to cubic YSZ, and coincide well with the ones reported in the JCPDS file No. 30–1468 for 8 mol % YSZ (8YSZ), which is purely cubic. The same is true for the VPS samples, which are of the same composition (6YSZ) [54]. A sample with 6.5 mol % YSZ was found to be purely cubic previously [12]. Consequently, no significant inherent conductivity difference (> factor 1.5) between 6YSZ and 8YSZ can be ascribed to a phase impurity.

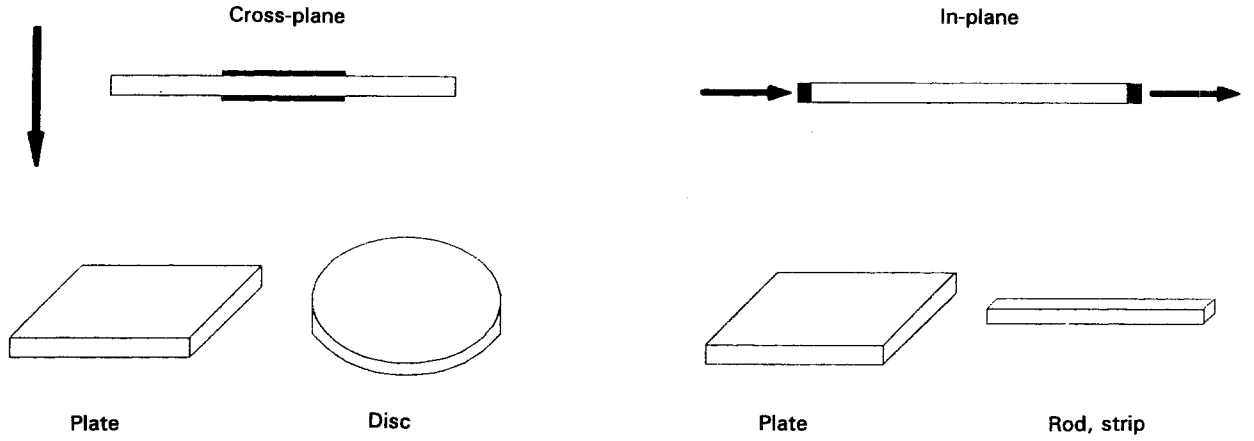

Figure 2 Definition of cross-plane and in-plane conductivity for the YSZ electrolyte samples.

TABLE III Origin, dimension and composition of the tested YSZ electrolyte samples. 6YSZ = 6 mol % YSZ; 8YSZ = 8 mol % YSZ

Electrolyte fabrication technique	Composition	Sample dimensions	Origin
HIP	6YSZ	Disc ϕ 25 mm, 2 mm thick or square 25 × 25 mm, 1 mm thick	Swiss Company
Tape-casting	8YSZ	Green tape cut to size, 180/250/300 μm thick	German company
VPS	6YSZ	Square 45 × 45 mm^2, 200 μm thick	Swiss company
Calendering	8YSZ	Square 45 × 45 mm^2, 200 μm thick	British university

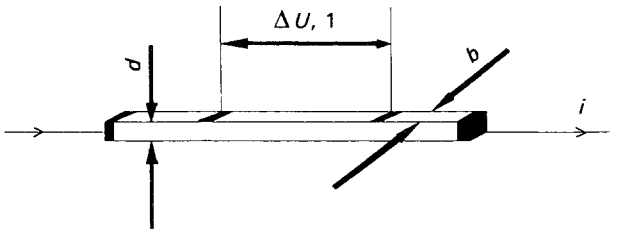

Figure 3 Principle of the four-point probe method.

2.1.2. Conductivity and composition

The conductivity of YSZ changes with dopant concentration [52, 55–57]. Ideally, the samples should be all of the same dopant concentration, in order to compare directly the different fabrication techniques. However, since the maximum conductivity of YSZ occurs at about 7 mol % Y_2O_3 concentration [52], the conductivities of 6YSZ and 8YSZ, as is the case for all our samples (see Table III), lie close to each other.

Thus, any significant difference (> factor 1.5) in conductivity observed between a sample of 6 mol % YSZ and sample of 8 mol % YSZ, cannot be ascribed to the difference in dopant concentration.

2.2. Conductivity measurement techniques

2.2.1. Four-point method

The principle of the four-point technique is sketched in Fig. 3. A rod (for thick samples, > 1 mm) or a strip (for thin samples, < 500 μm) of several centimetres long and about 2 mm wide was cut from the YSZ sample with a diamond saw [58]. Four Pt wires (0.25 mm) were attached with Pt-paste (Degussa 308 A) as in Fig. 3. For the outer contacts, Pt-paste was applied all around the edges of the strip or rod. On applying a constant current, i, through the two outer contacts, a voltage drop, ΔU, across the two inner contacts was recorded. For every temperature, four (current, voltage)-points were recorded. These four applied currents were chosen as $+i$, $+2.i$, $-i$ and $-2.i$, where i is of the order of 1 mA cm^{-2} so as not to cause any Joule heating effect which would influence the measurement. The four recorded voltage drops were then plotted versus the corresponding applied current values. Only when a straight line was obtained, was the resistance value, i.e. the slope of the straight line, accepted. For the geometry given in Fig. 3, the conductivity, σ, of the sample at each temperature was calculated through the formula

$$\sigma = 1/\rho = (i/\Delta U) \times (bd/l)$$

where ρ is the resistivity, b the breadth, d the diameter and l the length of the rod.

2.2.2. Impedance spectroscopy

For impedance measurements, two test electrodes of 1 cm^2 area were painted symmetrically on opposite sides of a planar sample. Two contact wires per electrode were attached with a metal binder paste. At each temperature, the frequency was swept typically from 20 kHz to 0.1 Hz to give a characteristic arc response in a Nyquist plot (imaginary part of the impedance plotted against its real part). This arc corresponds to the electrode reaction impedance. The experimental set-up is sketched in Fig. 4a [59].

At the high frequencies (limited to 20 kHz for FRA 1253), the arc intersects with the real axis. This value corresponds to the electrolyte resistance, R_{el}. For a given geometry, area $A = 1$ cm^2, measured thickness of the sample, d, the conductivity at a given temperature was derived as

$$\sigma = 1/\rho = (1/R_{el}) \times (A/d)$$

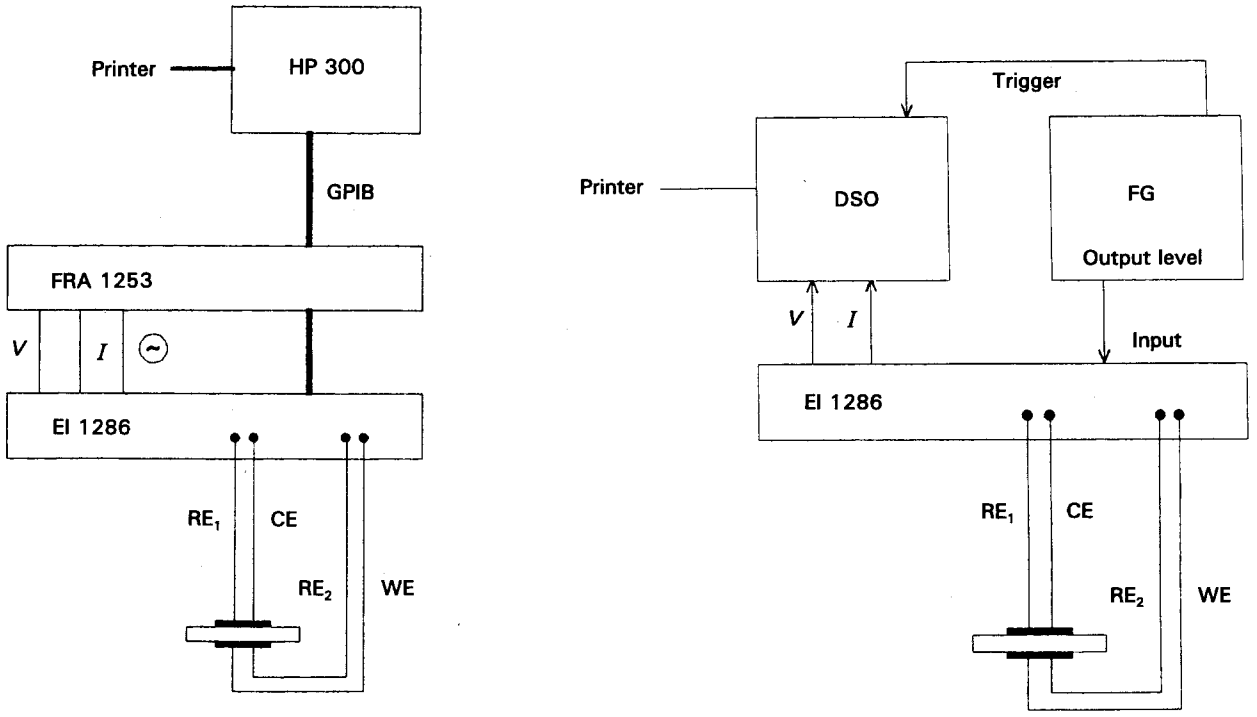

Figure 4 Experimental set-up for (a) impedance spectroscopy and (b) current-interruption technique. EI, Solartron electrochemieal interface 1286; FRA, Solartron frequency response analyser 1253; HP, Hewlett Packard series 300 computer; GPIB, Interface Bus; FG, Hewlett Packard function generator; DSO, Gould 1425 digital storage oscilloscope; RE_1, RE_2, CE, WE: reference, counter and working electrode connections, respectively.

Suitable equivalent electrical circuits for fitting experimental data are given elsewhere [58].

2.2.3. Current interruption technique

The principle of the current interruption technique, together with its drawbacks and advantages, is described elsewhere [58]. Samples were prepared in the same way as for an impedance measurement. The experimental set-up is sketched in Fig. 4b [60].

2.2.4. van der Pauw technique

The van der Pauw technique [61] is quick and easy to use, but has the disadvantage of only measuring the in-plane conductivity of the YSZ samples (Fig. 5).

A support plate with four contact points A–B–C–D arranged in a square geometry of $10 \times 10\ mm^2$, was pressed on a YSZ sample. A constant current was passed between pairs of points A and B, then B and C, and the resulting voltage drop measured across points D and C or A and D, respectively. The two obtained resistances, $R_1 = (\Delta U_{DC}/i_{AB})$ and $R_2 = (\Delta U_{AD}/i_{BC})$, allowed calculation of the conductivity of the underlying YSZ sample, with thickness d, through the approximated van der Pauw formula [61]

$$\sigma = \frac{1}{\rho} = \frac{\ln 2}{\pi d\,[(R_1 + R_2)/2]}$$

The support plate was made of stumatite [58], and the four contact points of silver paste to which silver wires were attached. The van der Pauw technique applied on YSZ has been shown to give the same resistivity values as determined from impedance spectroscopy [62].

Correction formulae, that take into account displacements of the contacts or that consider the finite size of the contacts, are available in the literature [63]. Deviations from the correct value due to these displacements can be very considerable [62].

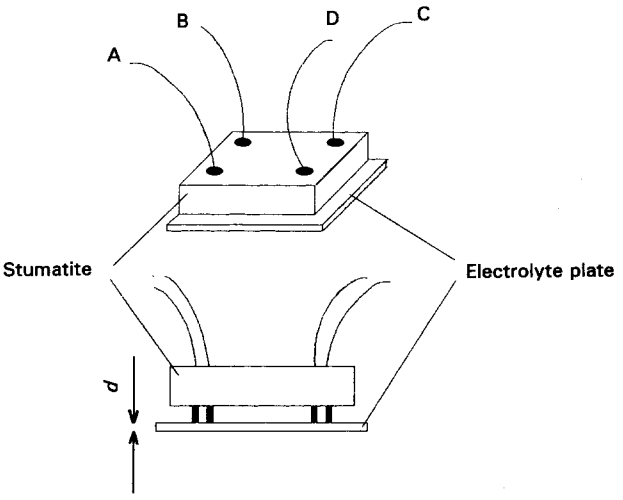

Figure 5 Set-up for the van der Pauw measurement. A support plate made of stumatite (alumino-silicate mineral) bearing four contact points, A–B–C–D, is pressed on a YSZ electrolyte plate.

The in-plane and cross-plane conductivities of all samples were measured between 400 and 900 °C at 12 different temperatures. The temperature was read from a thermocouple placed as close as possible (< 1 cm) to the sample. The constant heating zone of the oven (carbolite CSF 65 1000 $°C^{-1}$, tubular) was 20 cm.

3. Results

3.1. HIP samples

YSZ conductivity, σ_0, and activation energy E_A for the HIP samples were derived from an Arrhenius plot

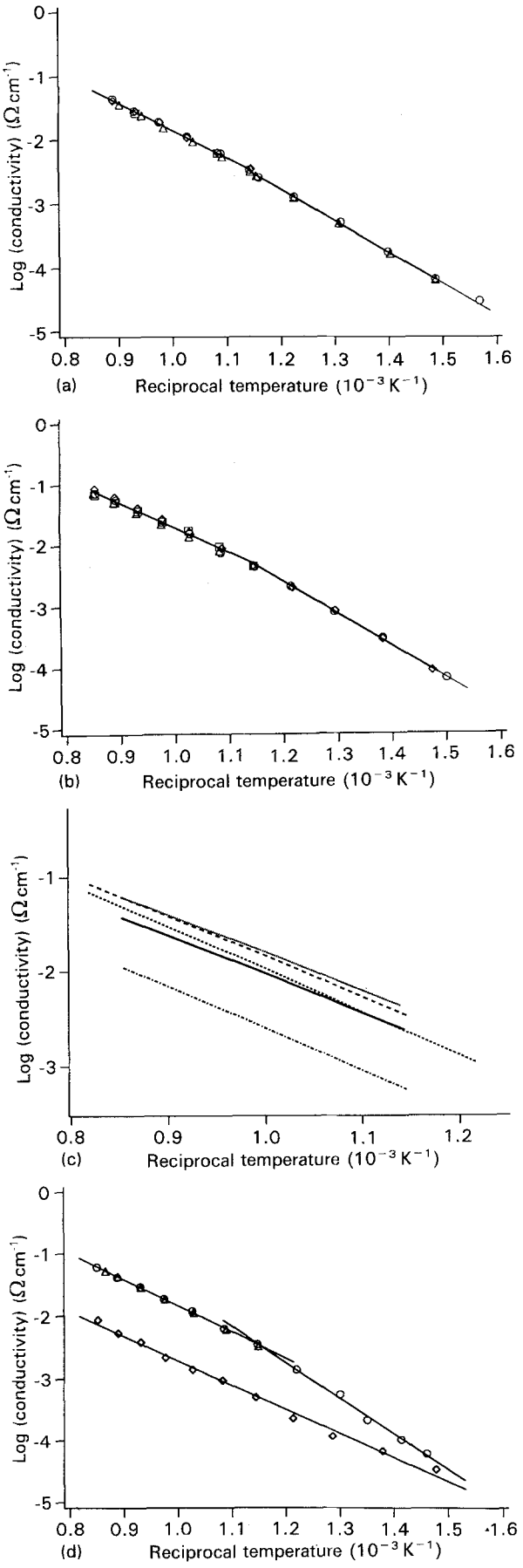

Figure 6 Arrhenius plot for the conductivity of YSZ electrolyte samples, fabricated by: (a) HIP, (b) tape casting, (c) VPS and (d) calendering. (a), (b): (△) four-point method; (○) impedance spectroscopy; (□) current-interruption technique; (◇) var der Pauw method; (c): (—) as sprayed, in-plane; (. . . .) sintered, in-plane; (– · – · –) as sprayed, cross-plane; (- - - -) sintered, cross-plane; (– – –) HIP 6YSZ; (d): (△) in-plane, sample A; (◇) cross-plane, sample A; and (○) cross-plane, sample B.

(Table IV)

$$\log \sigma = \log \sigma_0 - E_A/(RT)$$

as shown in Fig. 6a.

The measurements were performed on different samples from different batches. Excellent reproducibility was obtained. Fig. 6a also demonstrates the equivalence of all four conductivity measurement techniques outlined above. Since in-plane and cross-plane values are identical, the samples are consequently isotropic. An electron micrograph (Fig. 7a) of an HIP sample shows that the material is uniformly dense. Extension of the measurements to low temperatures reveals a break in the Arrhenius diagram at around 600 °C, confirmed by the appearance of a second arc in the impedance spectrum (Fig. 8). This behaviour is due to blocking of the conducting species at the grain boundaries of the sintered particles and has frequently been observed and explained elsewhere [64, 65]. The diameter of the high frequency arc in Fig. 8 represents the grain boundary resistance, R_{gb}, whereas R_{ig} denotes the intragrain resistance. The total resistance of the electrolyte is given by the sum of R_{gb} and R_{ig}. At the temperatures where SOFC are usually operated (> 800 °C), the grain boundary resistance is negligible.

3.2. Tape-cast samples

A similar result was obtained for thin 8YSZ samples fabricated by tape casting (Fig. 6b). Samples from different batches were tested to check for reproducibility. SEM pictures (Fig. 7b) show a minor closed porosity of the sintered samples, which, however, does not affect the isotropy: cross-plane and in-plane conductivities are identical. In absolute values, the tape-cast sample has a slightly higher conductivity than the hot pressed one.

3.3. Vacuum plasma sprayed samples

This type of sample (6YSZ) deviates from the expected behaviour, as observed with previous electrolyte samples. A strong anisotropy is reflected in the cross-plane conductivity values; these are several times lower than the in-plane conductivity values (Fig. 6c). Vacuum plasma sprayed zirconia is liable to be incompletely dense [17, 18, 21, 45, 50], which is confirmed by the porous structure observed by SEM (Fig. 7c), unless they are further heat-sintered to form denser layers. It is also reflected in the low power output of VPS based cells (see Fig. 1) and the low open circuit potential, which lies at around 0.9 V (see Table II). The possibility of conductivity anisotropy with a solid electrolyte like YSZ has been mentioned before [12, 62].

To confirm this point, a VPS sample was sintered at 1500 °C for 2 h. The sintering process changed the colour (from brownish-yellow to clear yellow) and the optical appearance (denser) of the sample. SEM pictures confirm that densification has taken place (Fig. 7d).

The conductivity anisotropy has virtually been eliminated after sintering (Fig. 6c). In-plane and cross-plane conductivity values differ on the average by no

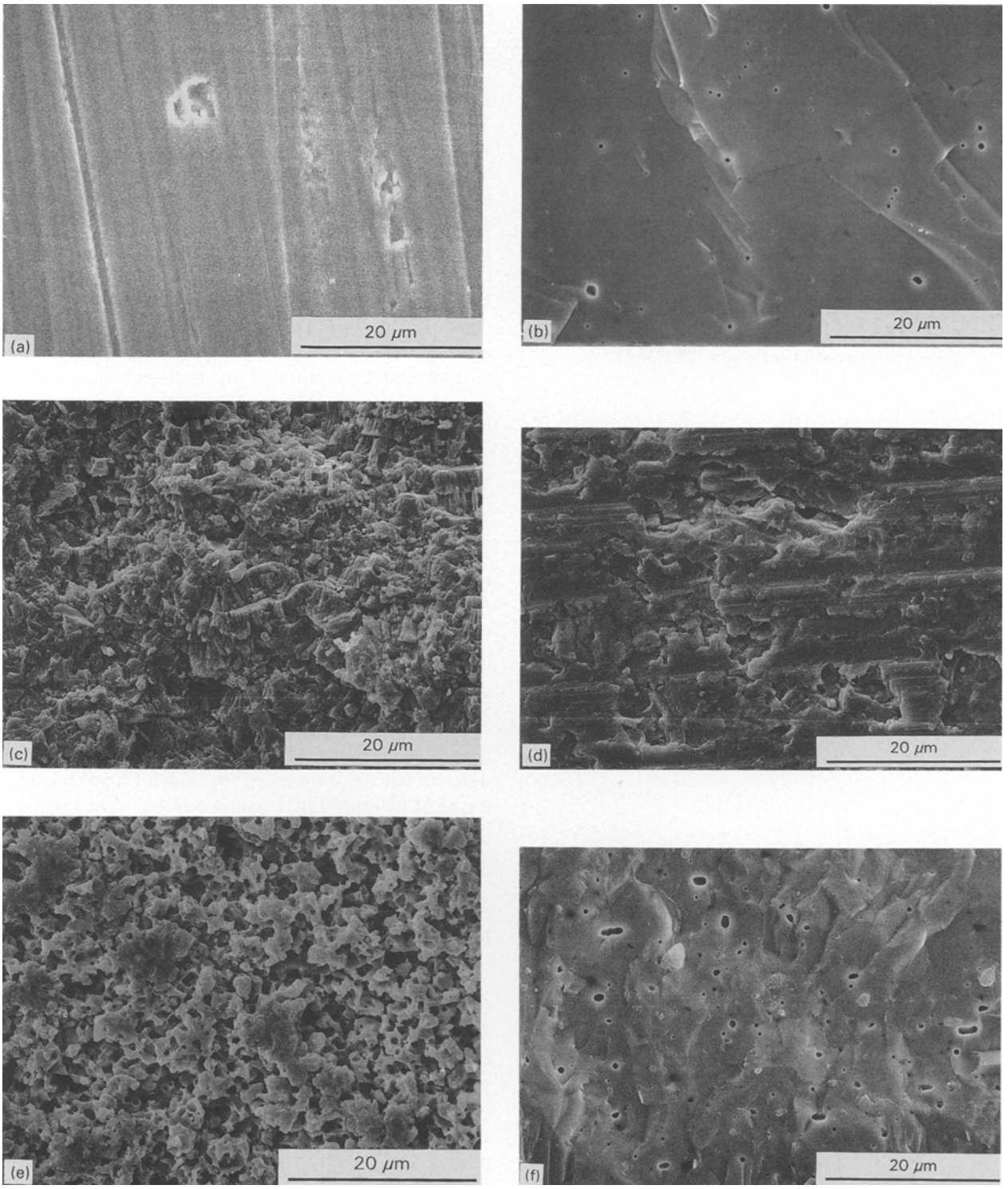

Figure 7 SEM micrographs of the YSZ electrolytes investigated in this study. Magnification × 2000. (a) HIP sample, top view; (b) tape-casted sample, edge view; (c) VPS sample, as sprayed, edge view; (d) VPS sample, sintered, edge view; (e) "badly" sintered calendered sample, edge view; and (f) "well" sintered calendered sample, edge view.

more than a factor of 1.3. Considering that all measurements are subjected to an error of about 20%, as error propagation calculation shows, this lies just within experimental error. In absolute terms, sintering has significantly improved the conductivity: an average 1.6 times and 5.8 times for the in-plane and cross-plane values, respectively (Fig. 6c). Resistivity values are given in Table IV. The fact that sintering densifies the sprayed electrolyte and thereby makes the conductivity equal to that of a HIP sample was reported before [56]. Also in this case, conductivity of the sintered VPS sample practically coincides with that of the HIP sample (Fig. 6c).

In an attempt to explain qualitatively and quantitatively these observations, a simple porosity model is proposed for the VPS electrolyte structure based on its fabrication procedure. To produce a 200 μm thick electrolyte, the plasma torch is moved back and forth 16 times, thus spraying one layer, L, of approximately 12 μm thickness, d, upon each passage. One such layer, L, in itself is fairly dense, as revealed by top view electron micrographs of the sprayed (without

TABLE IV Resistivity values (in Ω cm) of the VPS YSZ electrolyte. σ_o, pre-exponential Arrhenius factor; E_A, activation energy; F, average resistivity ratio as compared to the case "sintered, in-plane" (last column)

Temperature (°C)	Sprayed, cross-plane	Sprayed, in-plane	Sintered, cross-plane	Sintered, in-plane
800	202.2	56.8	47.0	34.0
850	132.6	38.4	30.4	23.2
900	90.1	26.8	20.4	16.3
950	63.2	19.3	14.2	11.8
1000	45.6	14.3	10.1	8.7
σ_o	64.8	118.1	373.0	171.9
E_A (eV)	0.876	0.815	0.904	0.802
F	5.87	1.63	1.33	1.00

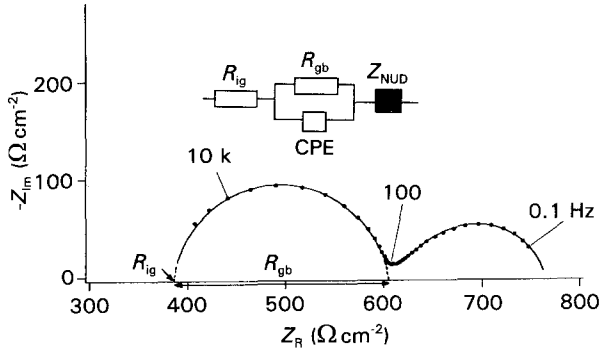

Figure 8 Impedance response with silver electrodes (2 cm^2) on a HIP YSZ electrolyte (2 mm thick) at $T = 440$ °C in air, and the corresponding fitting electrical circuit. CPE, constant phase element; Z_{NUD}, non uniform diffusion impedance; (●) experimental; (——) calculated.

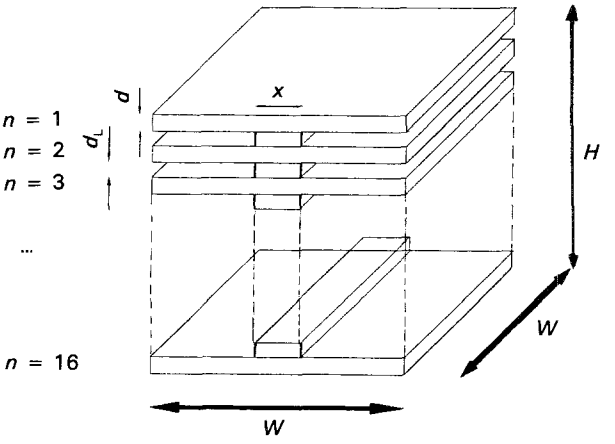

Figure 9 Model for the VPS electrolyte structure, based on its fabrication procedure. W, width and breadth of the sample; H, height (thickness); d, thickness of one sprayed layer (12 μm); d_L, width of the gap between two consecutively sprayed layers (variable); x, width of "connection bars" between consecutively sprayed layers (calculated).

sintering) sample. The VPS structure is consequently modelled as presented in Fig. 9.

It is suggested that the higher cross-plane resistance value (see Fig. 6c) is caused by weak contact between the individual layers, L, depicted in Fig. 9 as single bars (regrouping all single contact points between two layers, L) of width x; x being a fraction of the sample width, W, between 0 and 1. Each layer, L, was assumed to be dense. A sprayed structure has been recognized before as having a structure similar to the one proposed here [66].

This structure can be broken-up in a circuit of equivalent resistances in the case of current passing through the sample in the in-plane (Fig. 10a) and cross-plane (Fig. 10b) directions.

In Fig. 10, $R_a = \rho(W/Wd)$, $R_L = \rho(d_L/xW^2)$ and $R_b = \rho(d/W^2)$. ρ is set constant. After the sintering step, the structure is modelled as a densified plate of thickness

$$n\,d + (n-1)\,d_L\,x\,W^2/W^2$$

where the linking bars of thickness, d_L, and surface, $x\,W^2$, are all flattened out over a surface of W^2.

In the following manner, porosity was taken into account: since the volume, V, of the sample is W^2H, the porosity will be equal to

$$W(1-x)\,W d_L(n-1)/V$$

with an estimated porosity of 10% [67], this formula can inversely be used to calculate x.

The total resistance of the structure as sketched in Fig. 10a, b is calculated in a straightforward manner:

(a) cross-plane resistance (Fig. 10b): $R_{cross} = n\,R_b + (n-1)\,R_L$

(b) in-plane resistance (Fig. 10a): the circuit of Fig. 10a can be rearranged to an equivalent circuit that allows direct calculation of the total circuit resistance, which is denoted as R_{in}; this is outlined in the appendix.

R_{cross} and R_{in} are the experimentally measured cross-plane and in-plane resistances, from which, with the basic Pouillet formula, a value for the resistivity, ρ, is derived. Since initially a dense plate was assumed with area W^2 and thickness H, this derived resistivity is only apparent:

$$\rho_{cross,\ apparent} = R_{cross}(W^2/H)$$

$$\rho_{in,\ apparent} = R_{in}(H\,W/W)$$

These apparent resistivities are then related to the resistivity of the densely sintered material as the factors

$$F_{cross} = \rho_{cross,\ apparent}/\rho_{sintered}$$

and

$$F_{in} = \rho_{in,\ apparent}/\rho_{sintered}$$

These factors were computed, and found to be in good

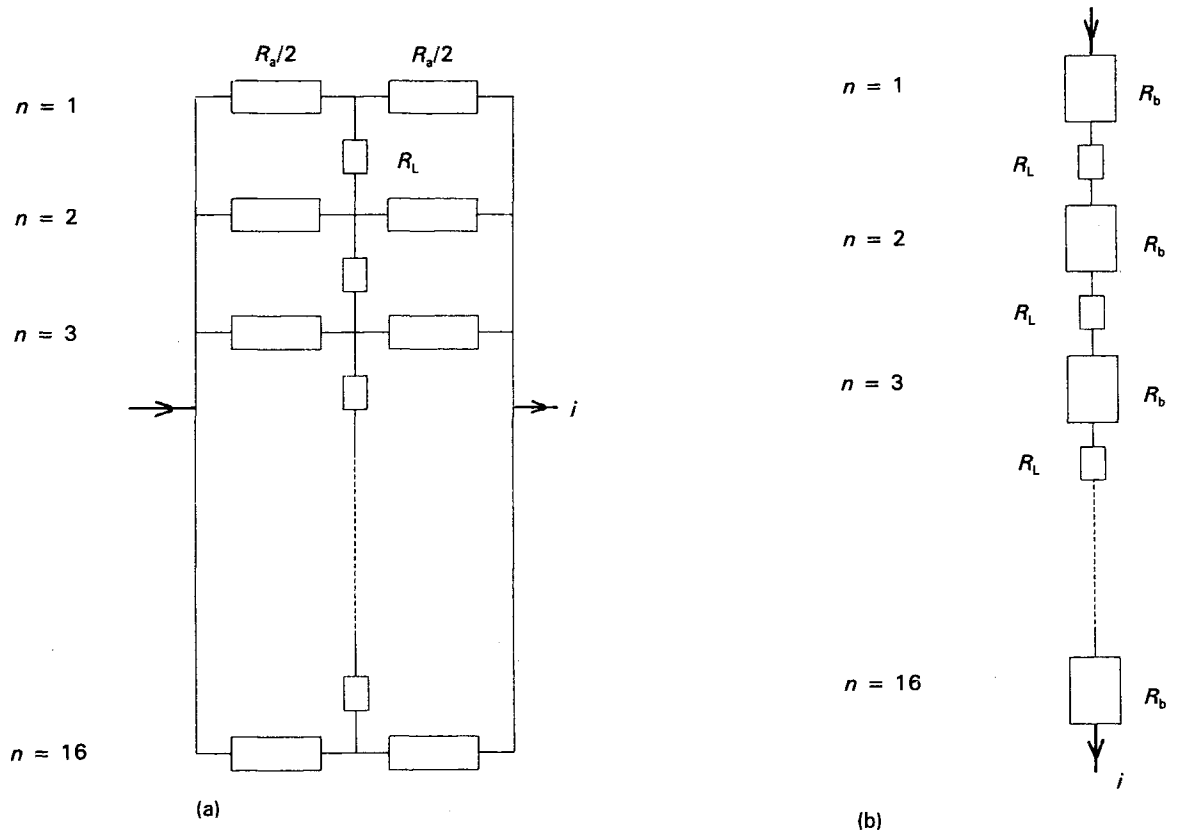

Figure 10 Equivalent resistance circuits for the VPS YSZ electrolyte model in Fig. 9, when current passes (a) in-plane and (b) cross-plane through the sample.

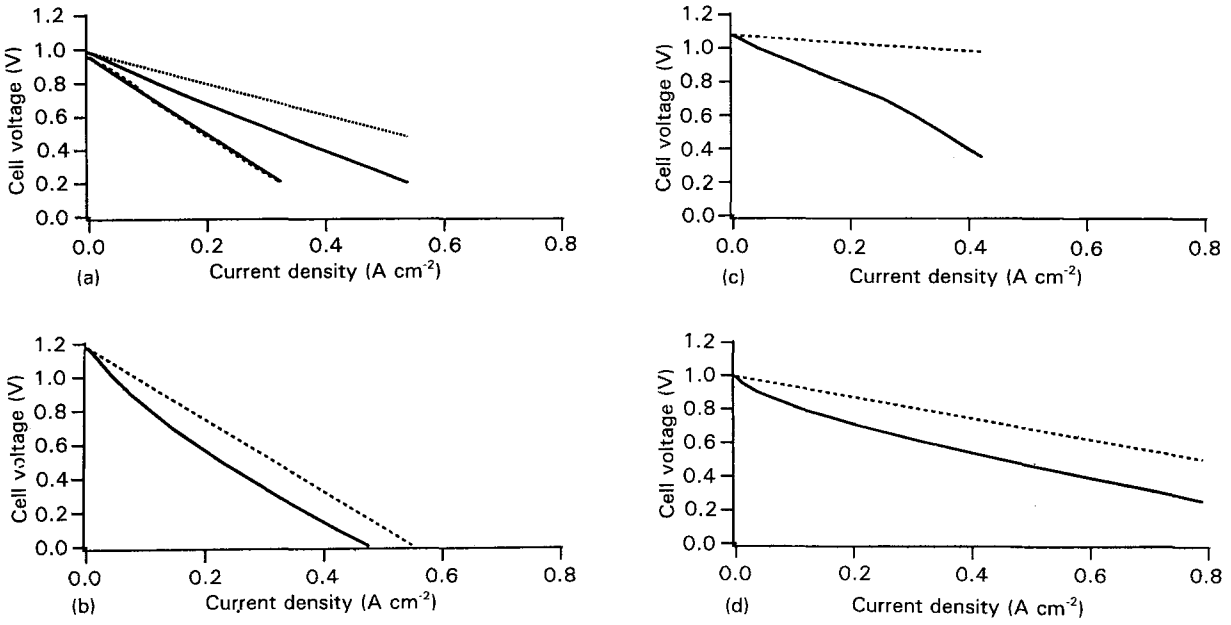

Figure 11 Current–voltage curves for the different YSZ electrolytes investigated in this study. The same electrode materials were used in all cases: Ni-cermet anode and (La,Sr) MnO_3 perovskite cathode. The dashed lines represent the iR drop of the cells. (a) VPS electrolyte (200 μm), pure starting powder (upper curve) and standard starting powder (lower curve), $T = 910\,°C$; (b) HIP electrolyte (1 mm) (Pt anode), $T = 925\,°C$; (c) tape-casted electrolyte (200 μm), $T = 910\,°C$; and (d) calendered electrolyte (200 μm), $T = 935\,°C$.

agreement with the experimentally observed factors F_{cross} and F_{in} (Table IV). For $W = 1$ cm and $\rho_{sintered} = 25\,\Omega$ cm (an average value, see Table IV), the best approximations to the experimentally observed ratios are: $F_{cross} = 5.93$ and $F_{in} = 1.39$. This occurs at an x-value of 0.0203, which means that the linking bars between the layers, L, in the model of Fig. 9 would extend to only 2% of the width of the sample.

In other words, the contacts between the individual sprayed layers, L, of the VPS sample seem, indeed, to be weak. Despite oversimplification of the model, it nevertheless illustrates the importance of non-porosity of the electrolyte sample.

The influence of impurities present in YSZ powder used for VPS was also studied. This was indirectly determined by comparing two identically sprayed

samples, one with a standard ($< 0.1\%$ Al_2O_3; $< 0.15\%$ SiO_2; $< 0.15\%$ TiO_2), and one with a pure starting YSZ powder ($< 0.01\%$ Al_2O_3; $< 0.05\%$ SiO_2; $< 0.05\%$ TiO_2) [68], as SOFC test cells. The i–V curves for both cells are given in Fig. 11a. With the standard powder, a maximum power of 95 mW cm^{-2} was obtained. Electrolyte resistivity was measured as 90 Ω cm, and constituted as much as 90% of the total loss. With the pure powder, the maximum power obtained at the same temperature was 165 mW cm^{-2}. Electrolyte resistivity in this case was measured as 40 Ω cm, and still contributed to over 2/3 of the total losses. Assuming an activation energy of 0.85 eV for VPS electrolyte resistivity (see Fig. 6c), an extrapolated power of around 250 mW cm^{-2} is calculated at 1000 °C. This value compares favourably with those reported in the literature for VPS cells (Table II). It again demonstrates the high potential of the technique, if the electrolyte resistance can be reduced. Acceptable resistivity values for the VPS YSZ electrolyte have been obtained before, e.g. 16 Ω cm at 1000 °C [47].

3.4. Calendered sample

With calendered samples, a similar behaviour to that with VPS samples was observed (Fig. 6d). Cross-plane conductivity was considerably lower than in-plane (Sample A in Fig. 6d), thereby suggesting mechanical imperfections in the electrolyte structure, in analogy to the VPS samples. It is interesting to note that cross-plane resistivity is a factor of about 6 times higher than the in-plane resistivity, which is very similar to the VPS case (see Table IV). SEM photographs indeed show open porosity within the electrolyte structure. Fig. 12 shows different sintering curves for the green calendered Samples A and B, and Fig. 7e and f the resulting structure as observed under the electron microscope. The corresponding conductivities for these different Samples A and B are represented in Fig. 6d. Again, a correlation between conductivity and electrolyte structure (porosity) is apparent. To obtain a dense sample, the sintering temperature profile of the green films is obviously crucial. A major difference between a tape-cast and a calendered sample is the higher green density of the latter, which makes its shrinkage upon sintering smaller. We found a linear shrinkage of 12% for the calendered and 24% for the tape cast films, which compares well with literature (16% and 25%, respectively, [51]). Therefore, different sintering profiles for these films are necessary. Indirect confirmation of this point was found by sintering a calendered green film according to the temperature profile for tape-cast films. The resulting plate showed a highly porous structure with no improvement in conductivity as compared to Sample A of Fig. 6d.

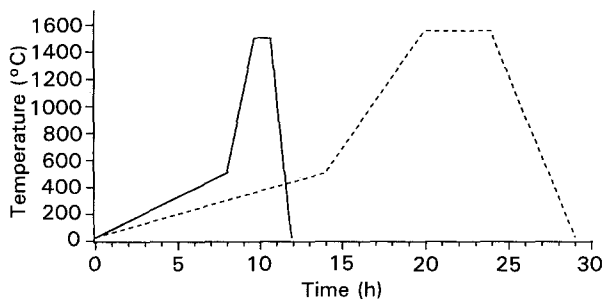

Figure 12 Different sintering temperature profiles for calendered green films: (——) sample A; (- - - -) sample B.

Data from our measurement ($\rho = 35$ Ω cm at 800 °C for Sample B) agreed well with that of calendered samples of the same origin reported in the literature ($\rho = 28$ Ω cm at 800 °C [12]).

3.5. Fuel cell tests

Cells with the different electrolytes used in this study, were tested for their output characteristics. An overview of the current–voltage characteristics obtained with these cells is given in Fig. 11. In all cases, the cathode was lanthanum strontium manganite ($La_{0.8}Sr_{0.2}MnO_3$), and the anode Ni-cermet (except in the case of Fig. 11b, where Pt was used as an anode). The cathode was supplied with air (1 l min^{-1}) and the anode with a 3% H_2O–H_2 mixture at a flow of 350 ml min^{-1}. The dashed lines represent the iR loss due to the electrolyte for each case. The cells were tested at temperatures between 900 and 940 °C. In Fig. 11a, showing the performance of two VPS cells, it was already stressed above that the electrolyte resistance was too high, considering the YSZ thickness, resulting in a low power output. In Fig. 11b, a cell with a 1.56 mm thick HIP electrolyte delivered over 100 mW cm^{-2} at 910 °C. Obviously, the electrolyte resistance accounts for nearly 80% of the losses in this case. For the cell with a tape-cast electrolyte (Fig. 11c), power output is still fairly low, but in this case was due to high electrode polarisation losses. The electrolyte loss amounts to only 20% of the total loss.

TABLE V Overview of (a) high and (b) low temperature resistivity values (in Ω cm) of the different YSZ electrolytes investigated. σ_0, pre-exponential Arrhenius factor; E_A, activation energy; (), extrapolated value

(a)

	HIP	Tape-casted	Calendered	VPS, sprayed	VPS, sintered
Temperature (°C)					
700	92.9	66.1	88.4		
800	35.7	26.6	35.2	202	47
900	16.3	12.5	16.4	90	20.4
1000	8.4	6.6	8.6	45.6	10.1
σ_0	283.5	261.2	223.7	64.8	373
E_A (eV)	0.853	0.818	0.829	0.876	0.904

(b)

	HIP		Tape-casted	Calendered	
	Total	Grain-boundary	Total	Total	Grain-boundary
Temperature (°C)					
400	15174	7970	12348	24604	5693
500	1709	413	1224	1872	169
600	318	42	206	257	(11)
E_A (eV)	0.978	1.326	1.036	1.155	1.577

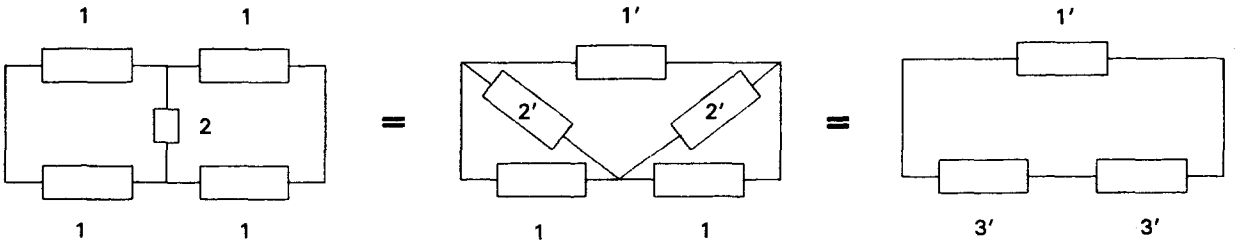

Figure 13 Rearrangement of the resistance circuit of Fig. 10a into an equivalent, calcuable circuit.

With other tape-cast electrolyte samples and more efficient electrodes, cells were developed delivering high power densities of over 500 mW cm^{-2} at 900 °C. The cell in Fig. 11d, with a calendered YSZ electrolyte of poor quality, delivered a fair power output of 230 mW cm^{-2} at 930 °C. The electrolyte, however, despite being thin (200 μm), was responsible for 65% of the total loss.

4. Conclusions

Conductivity measurements were performed by different techniques on yttria stabilized zirconia solid electrolyte samples of various origin. Table V gives an overview of the relevant parameters measured for the different samples.

Only in the case of complete density (HIP), or of minor closed porosity (tape-cast) of the electrolyte, are the samples isotropic and of good conductance. This implies the necessity of an additional sintering step for VPS sprayed samples (with a pure starting powder) and of a proper sintering procedure for calendered green films.

Appendix

To calculate the total resistance of the circuit given in Fig. 10a, use is made of the allowed rearrangement into an equivalent circuit as depicted in Fig. 13. Here

$$R_{1'} = (R_1^2 + 2R_1R_2)/R_2$$

$$R_{2'} = (R_1^2 + 2R_1R_2)/R_1$$

and

$$R_{3'} = (R_1R_{2'})/(R_1 + R_{2'})$$

This is iteratively calculated for every branch of the circuit from $n = 1$ to $n = 16$ (Fig. 10), and easily implemented into a computer program by means of a loop.

Acknowledgements

The support of the following people is appreciated: Mr J. Castano (Labo de Céramique, EPF Lausanne) for the SEM pictures of the tape-cast samples (Fig. 7b), Dr P. Debély and Dr B. Gut (EMPA, Switzerland) for the sintering curves of the calendered samples (Fig. 12), Dr H. Gruner for the VPS samples, and Dr H. Middleton (Imperial College, London) for introducing the current-interruption technique. The work was supported by the Swiss Federal Energy Office under the direction of Dr L. Dubal.

References

1. Proceedings of the International Symposium on Solid Oxide Fuel Cells, Nagoya, Japan, 13–14 November, 1989, edited by O. Yamamoto, M. Dokiya and H. Tagawa (Science House Coy. Ltd., Tokyo, 1989) pp. 1–37, 119–125.
2. Proceedings of the 2nd International Symposium on Solid Oxide Fuel Cells, Athens, Greece, 2–5 July, 1991, edited by F. Grosz, P. Zegers, S. C. Singhal and O. Yamamoto (Commission of European Communities) pp. 1–135, 167–205.
3. S. BARNETT, *Energy* **15** (1990) 1.
4. H. YAHIRO, Y. BABA, K. EGUCHI and H. ARAI, *J. Electrochem. Soc.* **135** (1988) 2077.
5. T. KENJO, S. OSAWA and H. MURAHASHI, *Denki Kagaku* **58** (1990) 533.
6. A. VIRKAR, *J. Electrochem. Soc.* **138** (1991) 1481.
7. Proceedings of the International Fuel Cell Conference, Makuhari, Japan, 3–6 February 1992 (New Energy and Industrial Technology Development Organisation, Tokyo) pp 289–357.
8. Fuel Cell Seminar, Tucson, USA 29 November–2 December 1992 Fuel Cell Seminar Organizing Committee (Commission of the European Communities, Japan Fuel Cell Development Center) pp. 237–269, 399–419, 510–528, 591–607.
9. H. ATKINSON and B. RICKINSON, in "Hot Isostatic Pressing", edited by J. Wood, (Adam Hilger Series, 1987).
10. J. HUIJSMANS, F. VAN HEUVELN, J. DE JONG and D. BOS, in Fuel Cell Seminar, Tucson, USA 29 November– 2 December 1992 (Fuel Cell Organizing Committee), p. 353.
11. I. YASUDA, T. KAWASHIMA, T. KOYAMA, Y. MATSUZAKI and T. HIKITA, *ibid.* p. 357.
12. F. POULSEN, J. BENTZEN and J. BILDE-SORENSEN, in Proceedings of the International Symposium on Solid Oxide Fuel Cells, Nagoya, Japan, 13–14 November, 1989, edited by O. Yamamoto, M. Dokiya and H. Tagawa (Science House Coy. Ltd., Tokyo, 1989). p. 93.
13. M. MORI, H. ITOH, N. MORI, C. ARAKAWA and T. ABE, in Proceedings of the 2nd International Symposium on Solid Oxide Fuel Cells, Athens, Greece, 2–5 July, 1991, edited by F. Grosz, P. Zegers, S. C. Singhal and O. Yamamoto (Commission of European Communities). p. 821.
14. T. IWATA and H. SHUNDO, in Fuel Cell Seminar, Tucson, USA, 29 November–2 December 1992 (Fuel Cell Organizing Committee), p. 289.
15. M. NAGATA, I. KAJI, S. YOSHIDA, N. KOBAYAHI, Y. SEINO and T. NAKAJIMA, in *ibid.* p. 305.
16. F. UMEMURA, H. OTA, K. AMANO, S. KANEKO, T. GENGO, S. UCHIDA, N. MURAKAMI and A. NOTOMI, in Proceedings of the International Symposium on Solid Oxide Fuel Cells, Nagoya, Japan, 13–14 November, 1989 edited by O. Yamamoto, M. Dokiya and H. Tagawa (Science House Coy. Ltd., Tokyo, 1989), p. 15.
17. H. SHUNDO, H. SHIMIZU, N. KUSUNOSE, T. IWATA, S. MARAYAMA and K. KOSEKI, in Proceedings of the 2nd International Symposium on Solid Oxide Fuel Cells, Athens, Greece, 2–5 July, 1991 edited by F. Grosz, P. Zegers, S. C. Singhal and O. Yamamoto (Commission of European Communities), p. 119.
18. H. ARAI, K. EGUCHI, T. SETOGUCHI, R. YAMAGUCHI, K. HASHIMOTO and H. YOSHIMURA, in *ibid.* p. 167.
19. I. KAJI, S. YOSHIDA, M. NAGATA, T. NAKAJIMA and Y. SEINO, in *ibid.* p. 221.
20. H. ARAI, K. EGUCHI, T. SETOGUCHI, H. ITOH and T. INOUE, in Proceedings Ist. International Symposium Solid Oxide Fuel Cells, Hollywood, FL, 16–18 October 1989, edited by S. C. Singhal (The Electrochemical Society) p. 288.
21. K. MASUMOTO, A. AYA and Y. MATSUI, in Proceedings

of the International Symposium on Solid Oxide Fuel Cells, Nagoya, Japan, 13–14 November, 1989, edited by O. Yamamoto, M. Dokiya and H. Tagawa (Science House Coy. Ltd., Tokyo, 1989), p. 145.
22. S. FUKAMI, M. KITOH, A. BUNYA, H. SAITOH, T. ITOH, Y. KAGA, Y. OHNO, K. EGUCHI and H. ARAI, in Proceedings of the 2nd International Symposium on Solid Oxide Fuel Cells, Athens, Greece, 2–5 July, 1991, edited by F. Grosz, P. Zegers, S. C. Singhal and O. Yamamoto (Commission of European Communities), p. 205.
23. N. NAKAGAWA, C. KURODA and M. IHIDA, in Proceedings of the International Symposium on Solid Oxide Fuel Cells, Nagoya, Japan, 13–14 November, 1989, edited by O. Yamamoto, M. Dokiya and H. Tagawa (Science House Coy. Ltd., Tokyo, 1989), p. 31.
24. E. THIELE, L. WANG, T. MASON and S. BARNETT, *J. Vac. Sci. Technol. A* **9** (1991) 3054.
25. NAKAGAWA, H. YOSHIOKA, C. KURODA and M. ISHIDA, *Solid State Ionics* **35** (1989) 249.
26. K. MYLES, in Proceedings of the 2nd International Symposium on Solid Oxide Fuel Cells, Athens, Greece, 2–5 July, 1991, edited by F. Grosz, P. Zegers, S. C. Singhal and O. Yamamoto (Commission of European Communities), p. 85.
27. K. KENDALL, in *ibid.* p. 429.
28. T. KUEPER, S. VISCO and L. DE JONGHE, *Solid State Ionics* **52** (1992) 251.
29. S. SINGHAL, in Proceedings of the 2nd International Symposium on Solid Oxide Fuel Cells, Athens, Greece, 2–5 July, 1991, edited by F. Grosz, P. Zegers, S. C. Singhal and O. Yamamoto (Commission of European Communities), p. 25.
30. H. SASAKI, M. SUZUKI, S. OTOSHI, A. KAJIMURA and M. IPPOMATSU, *J. Electrochem. Soc.* **139** (1992) L12.
31. K. DE VRIES, R. KUIPERS and L. DE HAART, in Proceedings of the 2nd International Symposium on Solid Oxide Fuel Cells, Athens, Greece, 2–5 July, 1991, edited by F. Grosz, P. Zegers, S. C. Singhal and O. Yamamoto (Commission of European Communities), p. 119.
32. R. FUKUDA, S. NAGAT, A. NEGISHI, Y. KASUGA and T. OKUO, in *ibid.* p. 193.
33. Z. OGUMI, Y. TSUJI, Y. UCHIMOTO and Z. TAKEHARA, in Proceedings of the International Symposium on Solid Oxide Fuel Cells, Nagoya, Japan, 13–14 November, 1989, edited by O. Yamamoto, M. Dokiya and H. Tagawa (Science House Coy. Ltd., Tokyo, 1989), p. 123.
34. *Idem.*, Proceedings of the 2nd International Symposium on Solid Oxide Fuel Cells, Athens, Greece, 2–5 July, 1991, edited by F. Grosz, P. Zegers, S. C. Singhal and O. Yamamoto (Commission of European Communities), p. 201.
35. T. SETOGUCHI, H. ITOH, M. SAWANO, K. EGUCHI and H. ARAI, in Proceedings of the International Symposium on Solid Oxide Fuel Cells, Nagoya, Japan, 13–14 November, 1989, edited by O. Yamamoto, M. Dokiya and H. Tagawa (Science House Coy. Ltd., Tokyo, 1989), p. 105.
36. K. EGUCHI, T. SETOGUCHI, H. ARAI, R. YAMAGUCHI and K. HASHIMOTO, in Fuel Cell Seminar, Tucson, 29 November-2 December 1992 (Fuel Cell Organising Committee) pp. 269.
37. K. EGUCHI, in "Proceedings of the IEA Workshop, Hertenstein, Switzerland, 24–29 June, 1990, p. 181.
38. T. SETOGUCHI, M. SAWANO, K. EGUCHI and H. ARAI, *Solid State Ionics* **40/41** (1990) 502.
39. K. TSUKUMOTO, F. UCHIYAMA, S. SHIRATORI, Y. OHNO and M. OKUTOMI, *Japan Spraying Assoc.* **24** (1987) 1245.
40. K. TSUKUMOTO, F. UCHIYAMA, Y. OHNO and Y. KAGA, *Surface Engineering* **6** (1990) 45.
41. H. NAKEGAWA, S. KOSUGE, H. TSUNEIZUNI, E. MATSUDA, H. MIHARA and Y. SATO, in Proceedings 1st. International Symposium Solid Oxide Fuel Cells, Hollywood, FL, 16–18 October 1989, edited by S. C. Singhal (The Electrochemical Society) p. 71.
42. T. SETOGUCHI, T. INOUE, H. TAKEBE, K. EGUCHI, K. MORINAGA and H. ARAI, *Solid State Ionics* **37** (1990) 217.
43. T. INOUE, T. SETOGUCHI, K. EGUCHI and H. ARAI, *ibid.* **35** (1989) 285.
44. V. VAN DIETEN, P. WALTERBOS and J. SCHOONMAN, in Proceedings of the 2nd International Symposium on Solid Oxide Fuel Cells, Athens, Greece, 2–5 July, 1991, edited by F. Grosz, P. Zegers, S. C. Singhal and O. Yamamoto (Commission of European Communities), p. 183.
45. H. ARAI, in Proceedings of the International Symposium on Solid Oxide Fuel Cells, Nagoya, Japan, 13–14 November, 1989, edited by O. Yamamoto, M. Dokiya and H. Tagawa (Science House Coy. Ltd., Tokyo, 1989), p. 9.
46. H. NAKEGAWA, S. KOSUGE, H. TSUNEIZUNI, E. MATSUDA, H. MIHARA and Y. SATO, in *ibid.* p. 125.
47. K. EGUCHI, T. SETOGUCHI, H. ITOH and H. ARAI, in 40th International Electrochemical Society Meeting, Kyoto, Japan, 17–22 September 1989, Extended Abstracts Vol 1, p. 362.
48. K. KINOSHITA, F. McLARNON and E. CAIRNS, "Fuel Cell Handbook" (US-DOE PUB-644, September 1988).
49. Proceedings of the Fifth IEA Solid Oxide Fuel Cells Workshop, an SOFC Materials, Process Engineering and Electrochemistry, Jülich, Germany, 2–4 March 1993, edited by P. Biedermann and B. Krahl-Urban (Forschungszentrum, Julich) pp. 167–206.
50. H. HAMATANI, T. OKADA and T. YOSHIDA, in Proceedings of the International Symposium on Solid Oxide Fuel Cells, Nagoya, Japan, 13–14 November, 1989, edited by O. Yamamoto, M. Dokiya and H. Tagawa (Science House Coy. Ltd., Tokyo, 1989), p. 119.
51. G. HEATH and R. SINGER, in Proceedings of the 2nd International Symposium on Solid Oxide Fuel Cells, Athens, Greece, 2–5 July, 1991, edited by F. Grosz, P. Zegers, S. C. Singhal and O. Yamamoto (Commission of European Communities), p. 55.
52. A. NAKAMURA and J. WAGNER, *J. Electrochem. Soc.* **133** (1986) 1542.
53. M. YOSHIMURA, *Amer. Ceram. Soc. Bull.* **67** (1988) 1950.
54. H. GRUNER, private communication.
55. R. MÄNNER, E. IVERS-TOFFE and W. WERSING, in Proceedings of the 2nd International Symposium on Solid Oxide Fuel Cells, Athens, Greece, 2–5 July, 1991, edited by F. Grosz, P. Zegers, S. C. Singhal and O. Yamamoto (Commission of European Communities), p. 715.
56. G. CHIODELLI, A. MAGISTRIS, M. SCAGLIOTTI and F. PARMIGIANI, *J. Mater. Sci.* **23** (1988) 1159.
57. H. TANNENBERGER, H. SCHACHNER and P. KOVACS, Jounées Int. d'Etudes des Piles à combustible, Brussels, June 1965, Revue EPE II **1** (1966) 19.
58. J. VAN HERLE and K. R. THAMPI, *J. Appl. Electrochem.*, in Press.
59. J. VAN HERLE, in "SOFC Micromodelling, an IEA Solid Oxide Fuel Cell Task Report", edited by L. Dubel (Swiss Federal office of Energy, Bern, Switzerland, 1992), p. 63.
60. H. MIDDLETON, Imperial College London, private communication.
61. L. van der PAUW, *Philips Research Reports* **13** (1958) 1.
62. F. POULSEN, P. BUITINK and B. MALMGREN-HANSEN, in Proceedings of the 2nd International Symposium on Solid Oxide Fuel Cells, Athens, Greece, 2–5 July, 1991, edited by F. Grosz, P. Zegers, S. C. Singhal and O. Yamamoto (Commission of European Communities), p. 755.
63. D. KOON, *Rev. Sci. Instrum.* **60** (1989) 271.
64. E. SCHOULER, PhD thesis, Inst. Nat. Polytechnique de Grenoble 1979.
65. H. BERNARD, PhD thesis, Inst. Nat. Polytechnique de Grenoble 1980.
66. Y. OHNO, Y. KAGA, A. MONMA, K. TSUKAMOTO, F. UCHIYAMA and T. OKUO, in Proceedings of the 2nd International Symposium on Solid Oxide Fuel Cells, Athens, Greece, 2–5 July, 1991, edited by F. Grosz, P. Zegers, S. C. Singhal and O. Yamamoto (Commission of European Communities), p. 455.
67. P. DEBÉLY, EMPA, Switzerland, private communication.
68. B. GUT, EMPA, Switzerland, private communication.

Received 11 August
and accepted 16 December 1993